A 1-D Model for the Millimeter-Wave Absorption and Heating of Dielectric Materials in Power Beaming Applications

Ian M. Rittersdorf, *Member, IEEE*, B. W. Hoff, *Senior Member, IEEE*, A. S. Richardson, S. A. Martin, V. V. Yakovlev, *Senior Member, IEEE*, P. S. Kim, and J. W. Schumer, *Senior Member, IEEE*

***Abstract*—A heat exchanger, based on a millimeter-wave absorbing ceramic composite, is under development. This article describes a 1-D finite-difference model that is used in the design of the heat exchanger. The purpose of this model is to offer a design tool that can rapidly estimate the overall performance of the heat exchanger. This fast model allows for absorber performance to be evaluated over a wide parameter space as opposed to 3-D finite-difference time-domain methods, which provide accurate results but require substantially more computational resources. The model enables quick calculations by approximating the electric field such that the simulation runs on the slower thermal dynamics time scale without having to resolve the faster electromagnetic time scale. Example calculations were performed to illustrate the performance of a realistic absorber. These calculations used experimentally measured material properties for a molybdenum-loaded aluminum nitride (AlN:Mo) ceramic composite. Simulation results show dielectric tiles reaching equilibrium temperature in around 20 s and the samples absorbing up to 70% of the power from the millimeter-wave beam. Parameter studies over Mo loading percentage and boundary condition temperatures highlight the complexity of this coupled system. An AlN:Mo composite with 3% Mo (by volume) exhibits uniform power absorption across multiple boundary condition temperatures and suggests robustness to variety of possible experimental testing conditions.**

***Index Terms*—Ceramic absorber, microwave power beaming, millimeter-wave, wireless power transfer.**

Manuscript received September 25, 2020; revised December 14, 2020; accepted December 30, 2020. Date of publication January 27, 2021; date of current version March 10, 2021. This work was supported by the Operational Energy Capability Improvement Fund. The work of B. W. Hoff was supported by the Air Force Office of Scientific Research under Grant FA9550-20RDCOR022. The works of S. A. Martin and V. V. Yakovlev were supported by the Air Force Research Laboratory, Leidos, Inc., under Grant P010200226. The review of this article was arranged by Senior Editor D. A. Shiffler. *(Corresponding author: Ian M. Rittersdorf.)*

Ian M. Rittersdorf, A. S. Richardson, and J. W. Schumer are with the U.S. Naval Research Laboratory, Washington, DC 20375 USA (e-mail: ian.rittersdorf@nrl.navy.mil).

B. W. Hoff is with the Air Force Research Laboratory, Albuquerque, NM 87123 USA.

S. A. Martin and V. V. Yakovlev are with the Worcester Polytechnic Institute, Worcester, MA 01609 USA.

P. S. Kim was with the Montgomery Blair High School, Silver Spring, MD 20901 USA. He is now with the University of Maryland, College Park, MD 20742 USA.

Color versions of one or more figures in this article are available at https://doi.org/10.1109/TPS.2021.3051108.

Digital Object Identifier 10.1109/TPS.2021.3051108

I. Introduction

WIRELESS power transfer is an attractive technology for situations where conventional power generation modalities are inaccessible. Decades of research and development have explored microwave wireless power transfer schemes utilizing RF rectifying diodes for conversion of electromagnetic radiation into electrical power [1]. However, another method discussed here employs the direct conversion of microwave radiation into heat to recapture the power. A project is underway to demonstrate the delivery of usable electrical power at distances approaching 1 km [2]. The demonstration will be conducted using a 95-GHz gyrotron transmitter and a microwave absorber coupled to a Stirling engine at the receiver for the generation of electricity. The design and manufacture of an efficient microwave absorbing heat exchanger in the millimeter-wave regime for the given source and beam efficiencies are paramount to achieve this goal.

A 3-D finite-difference time-domain (FDTD) model has been developed for this purpose [3], [4]. While this approach provides accurate results, it requires significant computational resources and performing significant amounts of simulations over a wide design parameter space becomes intractable. A 1-D model that captures the essential features of the heat exchanger system is outlined in this article. A single case with this 1-D model took 282 s on a 2.8-GHz, single-core laptop. A similar calculation performed in [3] took 1.5–6 h on a 28-core, 2.2-GHz workstation. This yields a speed-up of two to three orders of magnitude in CPU time. This model is appropriate for developing scaling relations and to test the material properties in the converter that optimize the conversion of millimeter-wave energy into heat to drive a Stirling engine.

Microwave heating has been the subject of research for decades [5] for a variety of fields such as materials processing [6]–[13], microwave assisted chemistry [14]–[17], food processing [18]–[23], and medical applications [24]–[26]. Fundamentally, the modeling techniques across all of these fields consists of treating the heated material as a lossy dielectric and coupling an electromagnetic solution to the heat equation through a heat source term. Such a multiphysics model is required to account for the temperature-dependent

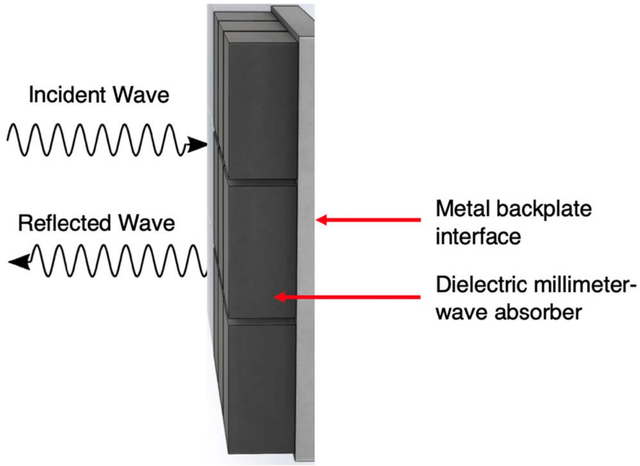

Fig. 1. Proposed design for a millimeter-wave absorbing heat exchanger. AlN:Mo composite ceramic tiles are mounted on a metal backplate that interfaces with a Stirling engine.

material properties of the dielectric that will change as heat is absorbed. This coupled system has been treated numerically in a variety of ways including finite-element methods (FEM) in 1-D [27], 2-D [28], and 3-D [13], [26], [29], as well as finite-difference method (FDM) in 1-D [30], 2-D [7], and 3-D [11], [12], [23], [31]–[33].

In the system under development, the lossy millimeter-wave absorber is mounted to a metal heat exchanger plate, as shown in Fig. 1. The incident wave originates from the millimeter-wave source, propagates through free space, and deposits energy within the dielectric in the form of heat. This heat is transported out of the dielectric through the heat exchanger and used to drive a Stirling engine. This article models a 1-D approximation to the power-delivery system by considering a plane-wave with normal incidence on a dielectric slab with a metal sheet attached to its back surface which models the heat exchanger. Dissipated power and temperature are computed with the use of a finite-difference scheme. These computations are based on experimental data of temperature-dependent electromagnetic and thermal material properties.

The remainder of this article is organized as follows. Section II discusses the specifics of the model. Section III looks at the material properties measurements of a recently published millimeter-wave absorbing ceramic composite and describes a sample calculation of a homogenous dielectric slab. Section IV discusses numerical results of over a single homogenous dielectric slab and a parameter space scan over boundary temperature and material properties. Finally, Section V concludes this article.

II. Model

The heat exchanger shown in Fig. 1 consists of multiple ceramic blocks stacked on the surface of a metal plate. In this design, thin air gaps are present between ceramic blocks in the array to allow for thermal expansion. This article, similar to [3], [4], is concerned with the performance of a single block of dielectric. In order to significantly reduce the calculation time required and allow for a much larger parameter space to be analyzed, the problem is reduced to 1-D, i.e., the block is considered infinite in the x- and y-directions. This will approximate the temperature along the center of the dielectric where thermal gradients at the edges of the material are negligible. This assumption should be valid for materials with sufficiently high thermal conductivities such as the ones studied here.

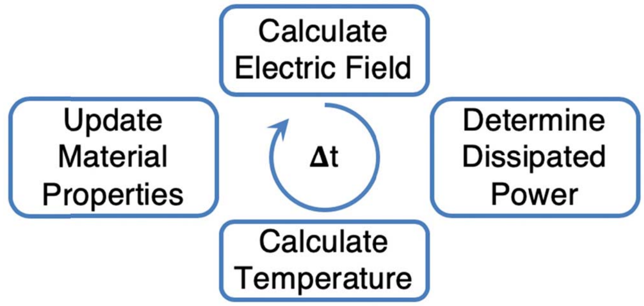

Fig. 2. Basic computational loop of the algorithm.

The two equations that need to be solved for this problem are the wave equation for the electromagnetic field in the dielectric, and the heat equation for the thermal response of the material to the energy deposited by the fields. Straightforward application of an FDTD method to this system would require time steps that are small enough to resolve the fastest dynamics, which in this case is the period of millimeter-wave oscillation. At 95 GHz, the required time step is a fraction of a wave period, or $\Delta t \lesssim 10^{-11}$ s. The timescale for the heat equation, on the other hand, is set by the thermal conductivity and specific heat of the heated material. For the materials considered in this article, the thermal timescale is on the order of a millisecond, which gives $\Delta t \lesssim 10^{-4}$ s. In order to avoid resolving the electromagnetic timescale, the material properties are assumed to be constant on the timescale of the wave oscillation. With this assumption, the wave equation transforms into a Helmholtz equation for the spatial variation of the wave. There are many ways to solve the Helmholtz equation; this article uses a method where the dielectric is decomposed into many thin slabs that are taken to be uniform. This is a variation of the method used in [34]–[38].

The basic algorithmic approach to solve this 1-D coupled electromagnetic-thermal problem can be seen in Fig. 2 and has been implemented in Python 3. Using the assumptions described in the previous paragraph, the Helmholtz equation for the electric field is solved for all positions z. The power dissipated in the dielectric, which is proportional to the square of the electric field, is then calculated and leads to an increment in temperature. Finally, the temperature-dependent material properties of the dielectric are updated based on the current temperature. A single time step, Δt, is composed of these four substeps, and the algorithm is repeated until the desired amount of time has passed.

Fig. 3 shows a representation of a single heat absorbing dielectric tile on a metal backplate. The tile has thickness L and is divided into M slabs of arbitrary thickness with $M + 1$ interfaces and is mounted to a metal plate at $z = L$,

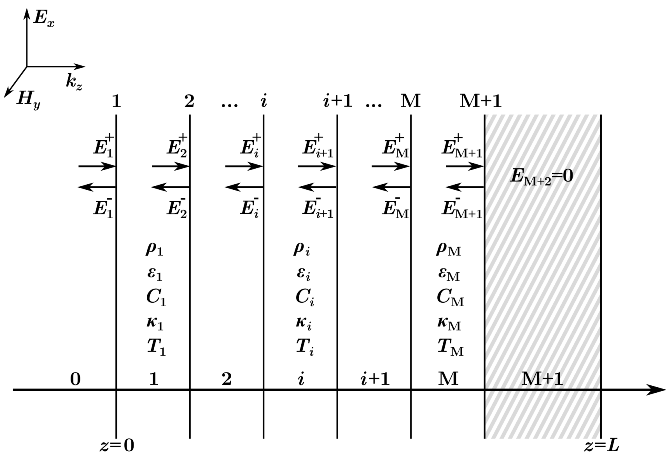

Fig. 3. One-dimensional model of a multilayer dielectric of thickness L mounted on a metal backplate. The total dielectric consists of M total layers and $M+1$ boundaries. Each layer has its own time-dependent temperature, temperature-dependent material properties, and electric field solutions.

labeled as the $(M+1)^{\text{th}}$ region. This multilayer approach is used to allow for spatial temperature variations to occur in the model. Each dielectric layer has electrical and thermal material properties that are functions of temperature T and thus will change as a function of time as microwave energy is absorbed and the system temperature increases. The electromagnetic properties of each dielectric layer are described by the complex permittivity, $\varepsilon(T) = \varepsilon'(T) - j\varepsilon''(T)$, where the real part ε' is the dielectric constant and the imaginary part ε'' is the loss factor related to the absorbed energy; heat is, therefore, deposited in this region by the microwaves if the dielectric is lossy, i.e., $\varepsilon'' \neq 0$. Each dielectric layer also has the temperature-dependent thermal properties of specific heat, $C_p(T)$, and thermal conductivity, $\kappa(T)$. The density, ρ, of each layer is assumed to be independent of temperature.

The incident wave originates from the source in free space. A reflection occurs at the surface of each dielectric layer due to a change in the index of refraction at that interface and E_i^+ and E_i^- are the amplitudes of the forward and reverse propagating electric field solutions on the left-hand side of the ith interface, respectively. The total field on the left-hand side of the ith interface is $E_i = E_i^+ + E_i^-$. Each slab i of thickness l_i is modeled with its own physical parameters, independent of its neighbors: permittivity, density, specific heat, and thermal conductivity, denoted by $\varepsilon_i, \rho_i, C_i$, and κ_i, respectively. Thus, in order to get finer spatial resolution of the problem, the number of layers can be increased. Since the layer thickness l_i can be of arbitrary size, many thin layers can be concentrated around regions of high gradients, should the problem require it.

The electromagnetic solution is formed by assuming a plane wave with $\exp(j\omega t - jkz)$ dependence impinging on a multilayer dielectric with normal incidence, where ω is the frequency and $k = \omega\sqrt{\varepsilon\mu}$ is the wavenumber. By assuming that the electric field solution traveling in the forward direction at the dielectric-metal boundary is unity, i.e., $E_{M+1}^+ = 1$, the relative solution for $E(z)$ can be determined by iterating backward through all of the layers [34], [37]. This iterative solution for $E(z)$ can be expressed by a system of equations written in matrix form as

$$\begin{bmatrix} 1 & 0 & a_1 & b_1 & & & & & & \\ 0 & 1 & c_1 & d_1 & & & & & & \\ & & 1 & 0 & a_2 & b_2 & & & & \\ & & 0 & 1 & c_2 & d_2 & & & & \\ & & & & \ddots & & \ddots & & & \\ & & & & & & 1 & 0 & a_{M-1} & b_{M-1} \\ & & & & & & 0 & 1 & c_{M-1} & d_{M-1} \\ & & & & & & & & 1 & 0 & a_M & b_M \\ & & & & & & & & 0 & 1 & c_M & d_M \end{bmatrix} \begin{bmatrix} E_1^+ \\ E_1^- \\ E_2^+ \\ E_2^- \\ \vdots \\ E_{M-1}^+ \\ E_{M-1}^- \\ E_M^+ \\ E_M^- \end{bmatrix} = \begin{bmatrix} 0 \\ \vdots \\ 0 \\ b_M - a_M \\ d_M - c_M \end{bmatrix} \tag{1}$$

where the constants in the $2M \times 2M$ matrix are defined as

$$\begin{aligned} a_i &= -\frac{1}{\tau_i}e^{jk_il_i} \\ b_i &= -\frac{r_i}{\tau_i}e^{-jk_il_i} \\ c_i &= -\frac{r_i}{\tau_i}e^{jk_il_i} \\ d_i &= -\frac{1}{\tau_i}e^{-jk_il_i}. \end{aligned} \tag{2}$$

The quantity r_i is the reflection coefficient, defined as $r_i = (\eta_i - \eta_{i-1})/(\eta_i + \eta_{i-1})$, where $\eta_i = \sqrt{\mu_0/\varepsilon_i}$ is the characteristic impedance of the ith layer, and $\tau_i = 1 + r_i$.

Once the solution for E from (1) is obtained, it is renormalized to the power of the microwave source

$$E_{\text{in}} = \sqrt{2P_{\text{in}}\eta_0} \tag{3}$$

where P_{in} is the input power (W/cm^2) and η_0 is the characteristic free-space impedance. The electric field solution from (1) is renormalized such that $E_1^+ = E_{\text{in}}$. The electromagnetic solution couples to the thermodynamic solution through the power dissipated in the dielectric. The power dissipated in each layer of the dielectric (W/cm^3) is proportional to ε_i'' and given by

$$P_{d,i} = \frac{1}{2}\omega\varepsilon_i''|E_i|^2. \tag{4}$$

The temperature as a function of time is determined from the 1-D heat transfer equation with a source term

$$\rho C\frac{\partial T}{\partial t} = \kappa\frac{\partial T^2}{\partial z^2} + P_d(z,t) \tag{5}$$

where T is the temperature and $P_d(z,t)$ is the power dissipated in the material at a depth z inside the dielectric as described by (4). This form of the heat equation is chosen because, for typical ceramic absorbers, κ varies slowly enough such that $(\partial\kappa/\partial z)(\partial T/\partial z) \ll \kappa(\partial^2 T/\partial z^2)$ and the $\partial\kappa/\partial z$ term can be ignored.

In order to solve (5) on the grid shown in Fig. 3, the forward finite-difference scheme is employed. The solution for T_i^{n+1} is

$$T_i^{n+1} = T_i^n + \frac{\Delta t}{\rho C_i^n}\left(\kappa_i^n\frac{T_{i+1}^n - 2T_i^n + T_{i-1}^n}{\Delta z^2} + P_{d,i}^n\right) \tag{6}$$

where i is the spatial index and n is the temporal index. The solution to (5) requires initial conditions and boundary conditions. The initial temperature is uniform everywhere, i.e., $T(z, 0) = T_0$. The initial temperature T_0 is considered the temperature that the Stirling engine is able to maintain on the heat exchanger backplate and will be referred to as the operating temperature. The boundary condition at $z = L$ uses the Dirichlet boundary condition fixed at the operating temperature, i.e., $T(L, t) = T_0$. The front face of the dielectric is subject to the Robin boundary condition

$$\frac{\partial T(0,t)}{\partial z} = \frac{h}{\kappa}(T_1 - T_{\text{ext}}) \tag{7}$$

where T_{ext} is the ambient air temperature and h (W/m^2/K) is the convective loss coefficient. In the case where $h \to 0$, which is assumed for the remainder of this article, this boundary condition becomes the Neumann boundary condition, i.e., zero heat flux and $\partial T(0, t)/\partial z = 0$. The temperature-dependent material properties of the dielectric are updated based on the current temperature, and the simulation clock is advanced by the time step Δt.

III. Absorbing Ceramic Composite–AlN:Mo

For the design of the millimeter-wave heat exchanger, a composite of aluminum nitride loaded with metallic molybdenum powder (AlN:Mo) has been chosen. This choice is motivated by its high thermal conductivity in the wide temperature range that is required of the heat exchanger during Stirling engine operation. However, in the millimeter-wave regime, aluminum nitride by itself is characterized by relatively low dielectric losses. Aiming to increase the absorptivity and find the material demonstrating the best performance, a series of AlN:Mo composite samples with an additive range of 0.25%–4% Mo (by volume) were produced for experimental testing. The electromagnetic properties [39], [40] and thermal properties [41] of this material have been measured; this experimental data have been numerically processed to make it available in the temperature range of interest, 25 °C–1000 °C [3].

Fig. 4 shows the temperature dependence of the real and imaginary parts of the complex permittivity for various Mo loadings at 95 GHz. As the Mo content increases, the imaginary permittivity increases drastically. Fig. 5 shows the temperature dependence of the specific heat and thermal conductivity of the AlN:Mo composite for various Mo loading percentages. The thermal conductivity can be seen to decrease with increased temperature, while the specific heat is increasing with increasing temperature. These properties have similar values for the different loading percentages, i.e., the addition of Mo does not significantly alter the thermal properties of the aluminum nitride [41]. Table I shows the density of the different composites as measured in [39] which is independent of temperature.

IV. Computational Results

An L = 10-mm-thick slab of 3% AlN:Mo was given an initial temperature of T_0 = 700 °C that was the same as the temperature of the metal backplate. The right-hand side boundary (z = 10 mm) was fixed at T_0, while the left-hand side boundary (z = 0 mm) used a zero heat-flux boundary condition, i.e., there were no convective losses (h = 0) and $\partial T/\partial z$ = 0. The block was uniformly divided into M= 100 slabs resulting in a spatial resolution of Δz = 0.1 mm. The time step for the problem was Δt = 0.1 ms. The input power from the microwave source was P_{in} = 100 W/cm^2 at a frequency of f = 95 GHz. The calculation was run for a total simulated time of 50 s. This typical case is selected for discussion because it is in the middle of the parameter space of interest and it features all of the physics behaviors present in the simulations.

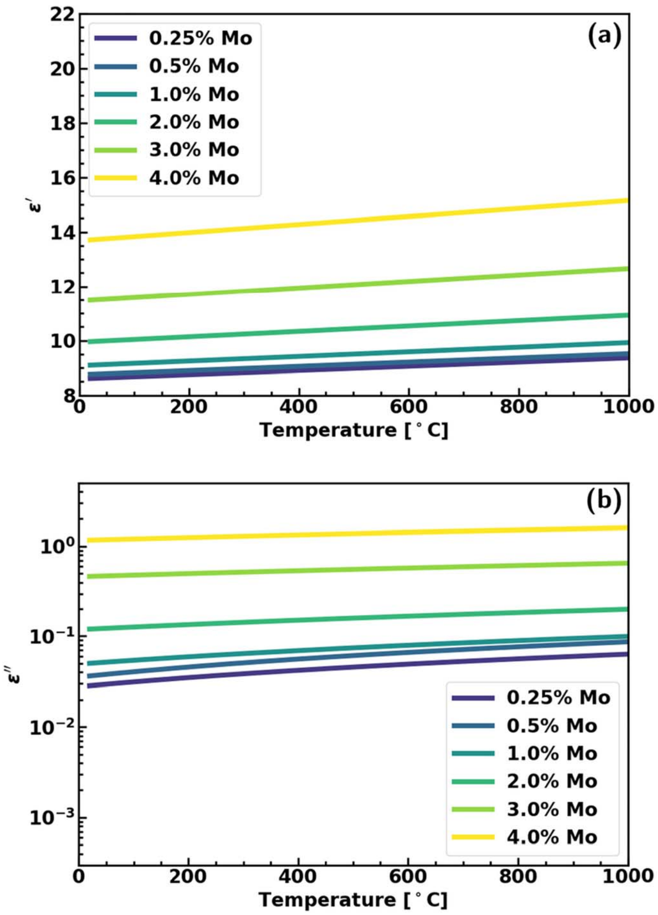

Fig. 4. (a) Real and (b) imaginary parts of complex permittivity of AlN:Mo composite loaded with various concentrations of Mo by volume at 95 GHz as a function of temperature [3].

TABLE I
Molybdenum-Loaded Aluminum Nitride Densities

Mo % (By Volume)	ρ (g/cm^3)
0.25	3.32
0.50	3.33
1.0	3.37
2.0	3.44
3.0	3.50
4.0	3.57

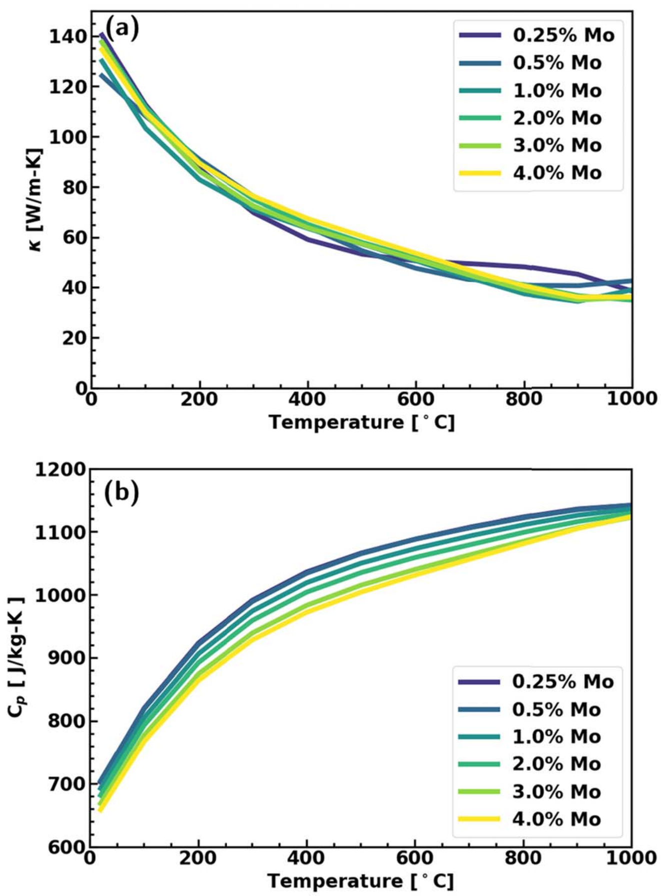

Fig. 5. (a) Specific heat and (b) thermal conductivity for AlN:Mo composite load with various concentrations of Mo by volume as a function of temperature [3].

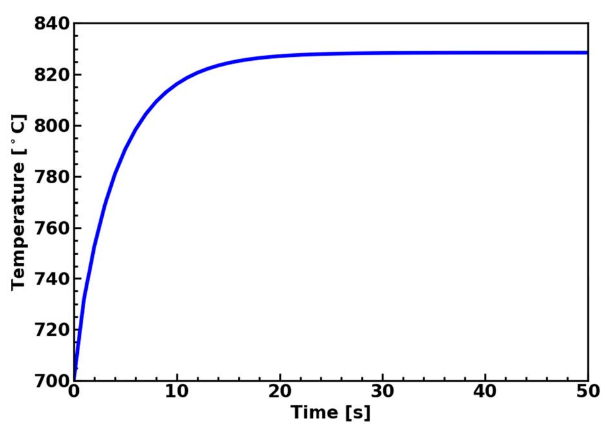

Fig. 6. Maximum temperature in the dielectric as a function of time; AlN:Mo with 3% Mo by volume, $T_0 = 700$ °C, $f = 95$ GHz, $P_{\text{in}} = 100$ W/cm^2, and $L = 10$ mm.

Fig. 6 shows the maximum temperature in the dielectric as a function of time. The maximum temperature can be seen to reach equilibrium after around 20 s at a temperature near 830 °C. The maximum always occurs on the front face of the dielectric, as can be seen in Fig. 7, showing the temperature profile, taken at time $t = 50$ s, with the highest temperature at $z = 0$ mm and with a nearly linear drop down to 700 °C.

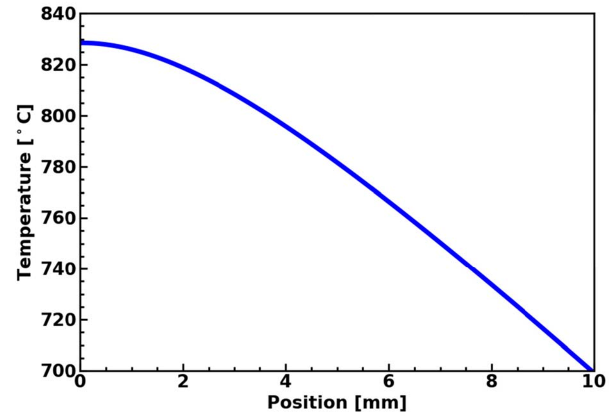

Fig. 7. Temperature in the dielectric as a function of position z at equilibrium ($t = 50$ s); AlN:Mo with 3% Mo by volume, $T_0 = 700$ °C, $f = 95$ GHz, $P_{\text{in}} = 100$ W/cm^2, and $L = 10$ mm.

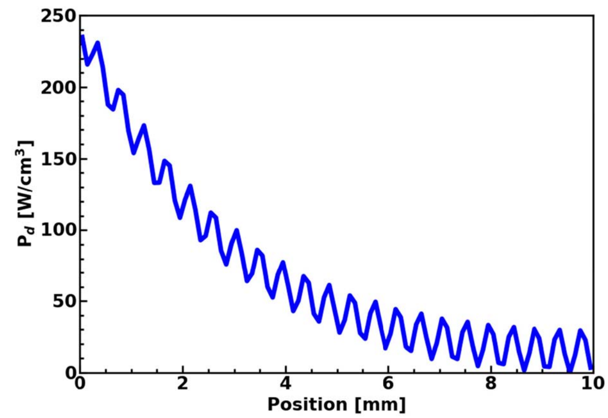

Fig. 8. Power dissipated in the dielectric as a function of position z at equilibrium ($t = 50$ s); AlN:Mo with 3% Mo by volume, $T_0 = 700$ °C, $f = 95$ GHz, $P_{\text{in}} = 100$ W/cm^2, and $L = 10$ mm.

Fig. 8 shows the power dissipation as function of z at equilibrium. The largest power dissipation corresponds to the highest temperature in the material and the oscillations have a wavelength of a 0.90 mm. This is the wavelength of a 95-GHz electromagnetic wave in a dielectric with $\varepsilon' \approx 12.4$, and the relative dielectric constant for AlN:Mo with 3% Mo by volume at 800 °C. By integrating over the curve shown in Fig. 8, the total power dissipated in the dielectric can be calculated. This allows the fractional absorbed power in the dielectric to be defined as

$$f_p = \frac{\int P_d dz}{P_{\text{in}}} \tag{8}$$

which describes how efficient the absorber is at capturing the incoming millimeter-wave beam. Fig. 9 shows fractional absorbed power as a function of time; it increases about 1.4% to reach an equilibrium value of $f_p = 0.68$ in around 10 s. This equilibration time corresponds to the knee in the temperature Fig. 6. The fractional absorbed power equilibrates faster than the temperature due to the coupled nature of the problem. The imaginary part of the dielectric constant varies slowly with temperature and as the temperature starts to change less rapidly, ε'' prime becomes roughly constant. The temperature

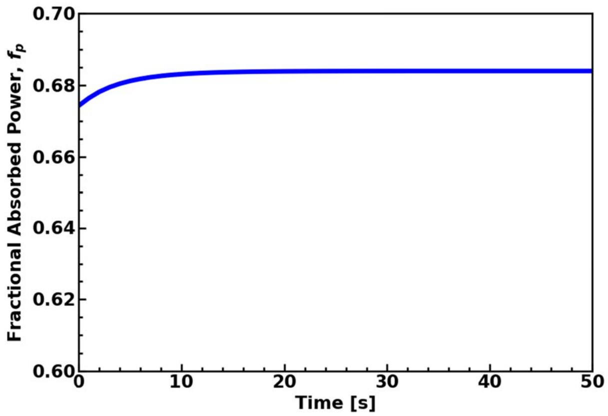

Fig. 9. Fractional absorbed power as a function of time; AlN:Mo with 3% Mo by volume, $T_0 = 700$ °C, $f = 95$ GHz, $P_{\text{in}} = 100$ W/cm^2, and $L = 10$ mm.

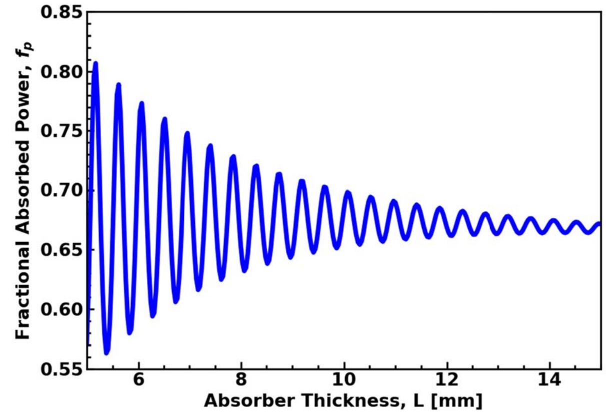

Fig. 11. Fractional absorbed power of the dielectric absorber temperature at equilibrium as a function of absorber thickness; AlN:Mo with 3% Mo by volume, $T_0 = 700$ °C, $f = 95$ GHz, and $P_{\text{in}} = 100$ W/cm^2.

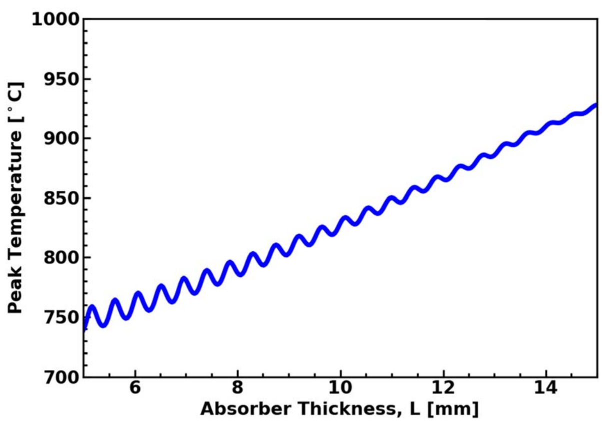

Fig. 10. Maximum dielectric temperature at equilibrium as a function of absorber thickness; AlN:Mo with 3% Mo by volume, $T_0 = 700$ °C, $f = 95$ GHz, and $P_{\text{in}} = 100$ W/cm^2.

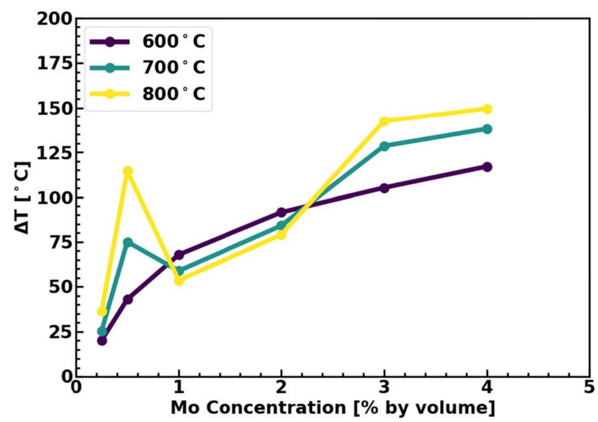

Fig. 12. Maximum temperature as a function of Mo loading for different operating temperatures; $L = 10$ mm, $P_{\text{in}} = 100$ W/cm^2, and $f = 95$ GHz.

takes additional time to equilibrate because even with a constant power absorption, it is still contending with heat loss through the $z = L$ boundary. The fractional absorbed power is the quantity of interest from the model outputs for making system-level efficiency calculations.

Calculations like the one described above were performed over the parameter space of operating temperature, Mo loading percentage, and absorber thickness in order to gain insight into how the absorber would perform over a range of power beaming demonstration operating conditions. Fig. 10 shows the peak equilibrium temperature as a function of absorber thickness for AlN:Mo with 3% Mo at an operating temperature of $T_0 = 700$ °C. The peak temperature is generally increasing as a function of thickness. The oscillatory structure superimposed on this linear increase is related to the wavelength of the $f = 95$ GHz signal inside the dielectric. The oscillatory behavior has a wavelength of 0.45 mm, exactly half the wavelength of 95 GHz in the medium. This factor of two arises from the metallic plate at the back boundary which causes the effective pathlength of the wave to be $2L$. Thicknesses exceeding 20 millimeters were not considered due to the fact that the equilibrium temperature rises above 1000 °C. It is desired to maintain the temperature reasonably below the limit at which the material may lose its robustness due to melting and this temperature represents the limit of material data available to the model.

Fig. 11 shows the fractional absorbed power as a function of length for the same Mo = 3% and $T_0 = 700$ °C case. It exhibits the same oscillatory behavior shown in Fig. 10 and oscillates about a central value of $f_p = 0.68$. The amplitude of oscillations decreases as the length of the absorbing composite increases. These oscillations have implications to the design of the absorber because a few hundred microns difference in length can result in a temperature change of 20 °C and a fractional absorbed power change of 10%–20%. Variations between each composite tile can be expected if the manufacturing tolerances of the absorbing composite production process are of this scale size or larger. This effect is likely to be diminished in 3-D simulations or in the experiment, where the beam might not impinge on the absorber with exact normal incidence and edge effects must be considered.

Fig. 12 shows how the peak material temperature scales with operating temperature. The largest changes in temperature occur at the higher operating temperatures. At $T_0 = 600$ °C, the peak temperature monotonically increases with Mo concentration. This differs from the cases of $T_0 = 700$ °C and $T_0 = 800$ °C operating temperatures, where there is a

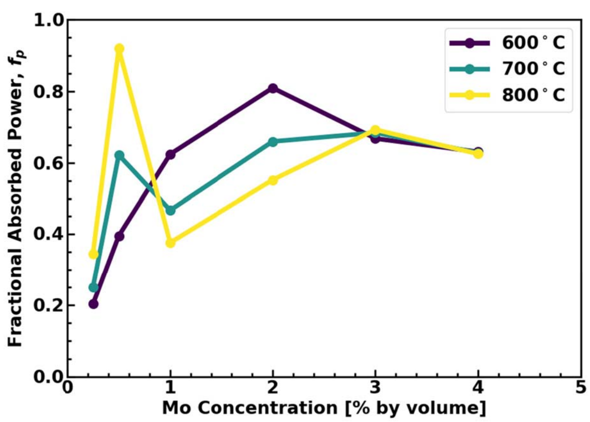

Fig. 13. Fractional absorbed power as a function of Mo loading for different operating temperatures; $L = 10$ mm, $P_{\text{in}} = 100$ W/cm^2, and $f = 95$ GHz.

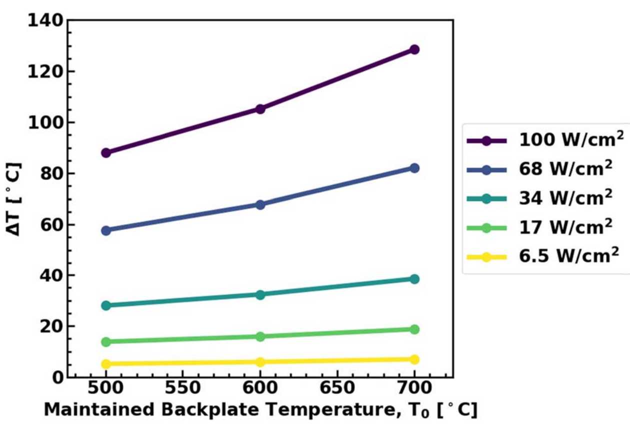

Fig. 14. Total temperature change ΔT across the dielectric as a function of operating temperature for various input power densities.

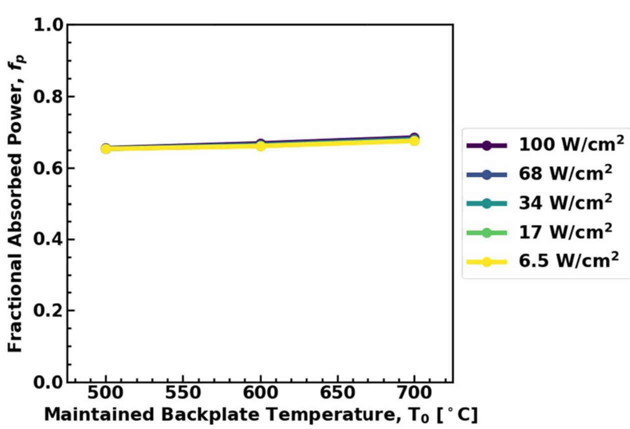

Fig. 15. Fractional absorbed power as a function of operating temperature for various input power densities.

local maximum at 0.5% Mo loading. This is likely explained by the behavior of fractional absorbed power, f_p, shown in Fig. 13, where f_p at Mo $= 0.5\%$ loading increases with increasing operating temperature. Dielectric losses increase with temperature, so the larger peak temperatures associated with larger T_0 leads to more millimeter-wave absorption and more power dissipated in the absorbing composite.

Figs. 14 and 15 show the temperature drop across the dielectric, ΔT, and the fractional absorbed power, f_p, respectively, for various operating temperatures and input power levels. Intuitively, ΔT increases with increased operating temperature and increased input power. The fractional absorbed power remains the same across all of these cases which is consistent with the fact that the material properties for the AlN:Mo composite do not change that much as a function of temperature. Similar to the results of [3], a material with 3% Mo concentration appears to be a promising demonstration candidate due to the uniform fractional power absorption across multiple operating temperatures and its robustness to a variety of possible experimental testing conditions.

V. Conclusion

A 1-D model that couples the absorption of millimeter-waves in a dielectric to the heat transfer for temperature-dependent materials was developed. The model was developed to allow for calculation over a large parameter space, in order to rapidly narrow design decisions, and offers an increase in speed of two to three orders of magnitude compared with corresponding 3-D calculations. Computational results show how maximum temperature and absorber efficiency scaled as a function of absorber length, temperature of the metal backplate, and material composition. An AlN:Mo ceramic composite with 3% Mo (by volume) at a thickness of 10 mm appears to meet the requirements of most likely candidate for a successful millimeter-wave power beaming demonstration. For this material and thickness, efficiencies for absorption of the incoming mm-wave radiation and subsequent conversion to heat were calculated to be around 66% for heat exchanger backplate temperatures ranging from 500 °C to 700 °C. The 1-D assumption of this model likely leads to optimistic values for fractional absorbed power, which is expected due to the anticipated reduced beam power coupling into the ceramic tile due to electromagnetic edge effects at the corners of the tiles as well as the 1-D heat transfer all acting to reduce the ceramic temperature. For the AlN:Mo composite materials studied here, a reduction in temperature results in reduced power absorption. The model is implemented in a general way that will allow for easily testing different absorber materials as well as implementing new thermal boundary conditions, such as time-evolving boundary conditions, which was beyond the scope of this article. The code could be paired with optimization techniques due to its low run times to make this a useful design tool in the future.

References

[1] W. C. Brown, "The history of power transmission by radio waves," *IEEE Trans. Microw. Theory Techn.*, vol. 32, no. 9, pp. 1230–1242, Sep. 1984, doi: 10.1109/TMTT.1984.1132833.

[2] B. W. Hoff *et al.*, "Millimeter wave interactions with high temperature materials and their applications to power beaming," in *Proc. 52nd IMPI's Microw. Power Symp.*, Long Beach, CA, Jun. 2018, pp. 82–83.

[3] P. Kumi, S. A. Martin, V. V. Yakovlev, M. S. Hilario, B. W. Hoff, and I. M. Rittersdorf, "Electromagnetic-thermal model of a millimeter-wave heat exchanger based on an AlN:Mo susceptor," *COMPEL Int. J. Comput. Math. Electr. Electron. Eng.*, vol. 39, no. 2, pp. 481–496, Jan. 2020, doi: 10.1108/COMPEL-07-2019-0271.

[4] P. Kumi, J. S. Venne, V. V. Yakovlev, M. S. Hilario, B. W. Hoff, and I. M. Rittersdorf, "Computational characterization of a composite ceramic block for a millimeter wave heat exchanger," in *Scientific Computing in Electrical Engineering*, G. Nicosia and V. Roman, Eds. Cham, Switzerland: Springer, 2020.

[5] J. M. Osepchuk, "A history of microwave heating applications," *IEEE Trans. Microw. Theory Techn.*, vol. 32, no. 9, pp. 1200–1224, Sep. 1984, doi: 10.1109/TMTT.1984.1132831.

[6] E. T. Thostenson and T.-W. Chou, "Microwave processing: Fundamentals and applications," *Compos. Part Appl. Sci. Manuf.*, vol. 30, no. 9, pp. 1055–1071, Sep. 1999, doi: 10.1016/S1359-835X(99)00020-2.

[7] J. Clemens and C. Saltiel, "Numerical modeling of materials processing in microwave furnaces," *Int. J. Heat Mass Transf.*, vol. 39, no. 8, pp. 1665–1675, May 1996, doi: 10.1016/0017-9310(95)00255-3.

[8] K. I. Rybakov, E. A. Olevsky, and E. V. Krikun, "Microwave sintering: Fundamentals and modeling," *J. Amer. Ceram. Soc.*, vol. 96, no. 4, pp. 1003–1020, Apr. 2013, doi: 10.1111/jace.12278.

[9] P. Rattanadecho, K. Aoki And, and M. Akahori, "Experimental validation of a combined electromagnetic and thermal model for a microwave heating of multi-layered materials using a rectangular wave guide," *J. Heat Transf.*, vol. 124, no. 5, pp. 992–996, Oct. 2002, doi: 10.1115/1.1495521.

[10] P. Rattanadecho, "The simulation of microwave heating of wood using a rectangular wave guide: Influence of frequency and sample size," *Chem. Eng. Sci.*, vol. 61, no. 14, pp. 4798–4811, Jul. 2006, doi: 10.1016/j.ces.2006.03.001.

[11] V. V. Yakovlev, S. M. Allan, M. L. Fall, and H. S. Shulman, "Computational study of thermal runaway in microwave processing of Zirconia," in *Microwave and RF Power Applications*. Toulouse, France: Cépaduès Éditions, 2011, pp. 303–306.

[12] E. M. Moon, C. Yang, and V. V. Yakovlev, "Microwave-induced temperature fields in cylindrical samples of graphite powder—Experimental and modeling studies," *Int. J. Heat Mass Transf.*, vol. 87, pp. 359–368, Aug. 2015, doi: 10.1016/j.ijheatmasstransfer.2015.02.021.

[13] C. Manière *et al.*, "Flash microwave pressing of Zirconia," *J. Amer. Ceram. Soc.*, vol. 103, no. 8, pp. 4110–4121, 2020, doi: 10.1111/jace.17072.

[14] S. A. Galema, "Microwave chemistry," *Chem. Soc. Rev.*, vol. 26, no. 3, pp. 233–238, Jan. 1997, doi: 10.1039/CS9972600233.

[15] I. Bilecka and M. Niederberger, "Microwave chemistry for inorganic nanomaterials synthesis," *Nanoscale*, vol. 2, no. 8, pp. 1358–1374, Aug. 2010, doi: 10.1039/B9NR00377K.

[16] E. Murphy and V. Yakovlev, "CAD technique for microwave chemistry reactors with energy efficiency optimized for different reactants," *Appl. Comput. Electromagn. Soc. J.*, vol. 25, pp. 1108–1117, Dec. 2010.

[17] C. Yang and V. V. Yakovlev, "An efficient empirical model for microwave-induced average temperature of liquid cylindrical reactants," *J. Microw. Power Electromagn. Energy*, vol. 47, no. 3, pp. 177–185, Jan. 2013, doi: 10.1080/08327823.2013.11689856.

[18] K. G. Ayappa, H. T. Davis, E. A. Davis, and J. Gordon, "Analysis of microwave heating of materials with temperature-dependent properties," *AIChE J.*, vol. 37, no. 3, pp. 313–322, Mar. 1991, doi: 10.1002/aic.690370302.

[19] W. Choi, S. H. Lee, C.-T. Kim, and S. Jun, "A finite element method based flow and heat transfer model of continuous flow microwave and ohmic combination heating for particulate foods," *J. Food Eng.*, vol. 149, pp. 159–170, Mar. 2015, doi: 10.1016/j.jfoodeng.2014.10.016.

[20] S. S. R. Geedipalli, V. Rakesh, and A. K. Datta, "Modeling the heating uniformity contributed by a rotating turntable in microwave ovens," *J. Food Eng.*, vol. 82, no. 3, pp. 359–368, Oct. 2007, doi: 10.1016/j.jfoodeng.2007.02.050.

[21] S. Ryynänen, "The electromagnetic properties of food materials: A review of the basic principles," *J. Food Eng.*, vol. 26, no. 4, pp. 409–429, Jan. 1995, doi: 10.1016/0260-8774(94)00063-F.

[22] S. Ryynänen, P. O. Risman, and T. Ohlsson, "Hamburger composition and microwave heating uniformity," *J. Food Sci.*, vol. 69, no. 7, pp. 187–196, May 2006, doi: 10.1111/j.1365-2621.2004.tb13619.x.

[23] T. Koutchma and V. Yakovlev, "Computer modeling of microwave heating processes for food preservation," in *Mathematical Analysis of Food Processing*. Boca Raton, FL, USA: CRC Press, 2010, pp. 625–658.

[24] M. Converse, E. J. Bond, S. C. Hagness, and B. D. Vanveen, "Ultrawide-band microwave space–time beamforming for hyperthermia treatment of breast cancer: A computational feasibility study," *IEEE Trans. Microw. Theory Techn.*, vol. 52, no. 8, pp. 1876–1889, Aug. 2004, doi: 10.1109/TMTT.2004.832012.

[25] Y. Lu, J. Ying, T.-K. Tan, and K. Arichandran, "Electromagnetic and thermal simulations of 3-D human head model under RF radiation by using the FDTD and FD approaches," *IEEE Trans. Magn.*, vol. 32, no. 3, pp. 1653–1656, May 1996, doi: 10.1109/20.497572.

[26] A. Sekkak, V. N. Kanellopoulos, L. Pichon, and A. Razek, "A thermal and electromagnetic analysis in biological objects using 3D finite elements and absorbing boundary conditions," *IEEE Trans. Magn.*, vol. 31, no. 3, pp. 1865–1868, May 1995, doi: 10.1109/20.376401.

[27] Y. Alpert and E. Jerby, "Coupled thermal-electromagnetic model for microwave heating of temperature-dependent dielectric media," *IEEE Trans. Plasma Sci.*, vol. 27, no. 2, pp. 555–562, Apr. 1999, doi: 10.1109/27.772285.

[28] L. E. Lagos, W. Li, M. A. Ebadian, T. L. White, R. G. Grubb, and D. Foster, "Heat transfer within a concrete slab with a finite microwave heating source," *Int. J. Heat Mass Transf.*, vol. 38, no. 5, pp. 887–897, Mar. 1995, doi: 10.1016/0017-9310(94)00200-F.

[29] A. A. Rabello, E. J. Silva, R. R. Saldanha, C. Vollaire, and A. Nicolas, "Adaptive time-stepping analysis of nonlinear microwave heating problems," *IEEE Trans. Magn.*, vol. 41, no. 5, pp. 1584–1587, May 2005, doi: 10.1109/TMAG.2005.845034.

[30] C. Liu and D. Sheen, "Analysis and control of the thermal runaway of ceramic slab under microwave heating," *Sci. China Ser. E, Technol. Sci.*, vol. 51, no. 12, pp. 2233–2241, Dec. 2008, doi: 10.1007/s11431-008-0221-7.

[31] L. Ma *et al.*, "Experimental validation of a combined electromagnetic and thermal FDTD model of a microwave heating process," *IEEE Trans. Microw. Theory Techn.*, vol. 43, no. 11, pp. 2565–2572, Nov. 1995, doi: 10.1109/22.473179.

[32] F. Torres and B. Jecko, "Complete FDTD analysis of microwave heating processes in frequency-dependent and temperature-dependent media," *IEEE Trans. Microw. Theory Techn.*, vol. 45, no. 1, pp. 108–117, Jan. 1997, doi: 10.1109/22.552039.

[33] R. Suga, O. Hashimoto, R. K. Pokharel, K. Wada, and S. Watanabe, "Analytical study on change of temperature and absorption characteristics of a single-layer radiowave absorber under irradiation electric power," *IEEE Trans. Electromagn. Compat.*, vol. 47, no. 4, pp. 866–871, Nov. 2005, doi: 10.1109/TEMC.2005.854102.

[34] S. J. Orfanidis, "Multilayer structures," in *Electromagnetic Waves and Antennas*. New Brunswick, NJ, USA: Rutgers Univ., [Online]. Available: http://eceweb1.rutgers.edu/~orfanidi/ewa

[35] R. E. Collin, *Foundations for Microwave Engineering*, 2nd ed. Hoboken, NJ, USA: Wiley, 2001.

[36] R. C. Nesnidal and T. G. Walker, "Multilayer dielectric structure for enhancement of evanescent waves," *Appl. Opt.*, vol. 35, no. 13, pp. 2226–2229, May 1996, doi: 10.1364/AO.35.002226.

[37] G. A. Kriegsmann and B. S. Tilley, "Microwave heating of laminate panels," *J. Eng. Math.*, vol. 44, no. 2, pp. 173–198, Oct. 2002, doi: 10.1023/A:1020868129550.

[38] H. Oraizi and M. Afsahi, "Analysis of planar dielectric multilayers as FSS by transmission line transfer matrix method (Tltmm)," *Prog. Electromagn. Res.*, vol. 74, pp. 217–240, 2007, doi: 10.2528/PIER07042401.

[39] B. W. Hoff *et al.*, "Characterization of AlN-based ceramic composites for use as millimeter-wave susceptor materials at high temperature: Dielectric properties of AlN:Mo with 0.25 vol% to 4.0 vol% mo from 25 to 550 °C," *J. Mater. Res.*, vol. 34, no. 15, pp. 2573–2581, Aug. 2019, doi: 10.1557/jmr.2019.177.

[40] M. S. Hilario *et al.*, "*W*-band complex permittivity measurements at high temperature using free-space methods," *IEEE Trans. Compon., Packag., Manuf. Technol.*, vol. 9, no. 6, pp. 1011–1019, Jun. 2019, doi: 10.1109/TCPMT.2019.2912837.

[41] B. W. Hoff *et al.*, "Characterization of AlN-based ceramic composites for use as millimeter wave susceptor materials at high temperature: High temperature thermal properties of AlN:Mo with 0.25% to 4.0% mo by volume," *MRS Adv.*, vol. 4, no. 27, pp. 1531–1542, 2019, doi: 10.1557/adv.2019.142.